RadoNorm
Managing risks from radon and NORM

Deliverable 3.3: Report on dose assessment for specific subgroups of the population

Work Package 3

This project has received funding from the Euratom research and training programme 2019-2020 under grant agreement No 900009.

Document information

Project Acronym	**RadoNorm**
Project Title	**Towards effective radiation protection based on improved scientific evidence and social considerations - focus on radon and NORM**
Project Type	**RIA**
EC grant agreement No.	**900009**
Project starting / end date	**1st September 2020 – 31 August 2025**
Work Package No.	**WP3**
Work Package Title	**Dosimetry**
Deliverable No.	**D3.3**
Deliverable Title	**Report on dose assessment for specific subgroups of the population**
Lead Beneficiary	**HUN-REN Centre for Energy Research**
Contractual Delivery Date	**28th February 2025**
Actual Delivery Date	**28th February 2025**
Type	**Report**
Dissemination level	**Public**
Authors	**Ämilie Louize Degenhardt (BfS), Árpád Farkas (HUN-REN EK), Péter Füri (HUN-REN EK), Augusto Giussani (BfS), Werner Hofmann (Paris-Lodron University of Salzburg), Balázs Madas (HUN-REN EK), Vladimir Spielmann (BfS).**

To be cited as:

Degenhardt Ä. L., Farkas Á., Füri P., Giussani A., Hofmann W., Madas B., Spielmann V. (2025): Report on dose assessment for specific subgroups of the population. Final version as of 28.02.2025 of deliverable D3.3 of project RadoNorm.

Disclaimer

Acknowledgement

This document is a deliverable of the RadoNorm project. This project has received funding from the Euratom research and training programme 2019-2020 under grant agreement No 900009.

Status of deliverable		
	By	Date
Delivered (Lead Beneficiary)	HUN-REN Centre for Energy Research	27th February 2025
Verified (WP Leader)	HUN-REN Centre for Energy Research	27th February 2025
Reviewed (Reviewers)	HUN-REN Centre for Energy Research, BfS	28th February 2025
Approved (PC)	PC (BfS)	28th February 2025
Submitted to EC (PC)	PC (BfS)	28th February 2025

Executive Summary

The assessment of radiation doses in specific subpopulations is crucial for refining radiation protection strategies. Task 3.3 of the RadoNorm project focused on developing advanced dosimetric models for three groups with potentially higher sensitivity to radiation exposure: embryos and foetuses, children, and individuals with severe asthma. These models account for age- and health-related variations that influence the uptake, distribution, and retention of radionuclides, particularly radon and its progeny.

A biokinetic model for pregnancy was developed to assess the maternal-to-foetal transfer of radon and its progeny. The model introduced new compartments for the placenta and foetal organs, considering gestational changes in tissue masses and blood flows. Findings indicate that direct radon transfer to foetal tissues is limited, but its progeny—particularly lead and polonium—may contribute more significantly to foetal radiation burden. The foetal liver was identified as the primary site of radon accumulation, while red bone marrow may experience prolonged exposure due to lead retention. These results improve dose estimations for the unborn child and support better risk assessment frameworks.

For children, numerical dosimetry models incorporating age-specific airway geometry and breathing rates were developed to evaluate radon progeny deposition in the lungs. Results indicate that smaller airway dimensions and thinner mucus layers lead to higher absorbed doses in basal and secretory cell nuclei, despite lower total deposition compared to adults. Given that these cells are targets for radiation-induced lung cancer, the findings highlight the need for age-specific risk assessments. Standard adult-based models may underestimate radiation risks in children, emphasising the importance of incorporating paediatric-specific parameters into dosimetric calculations.

For individuals with severe asthma, computational airway models were used to assess the impact of airway constriction and altered mucus dynamics on radionuclide deposition and clearance. Narrowed airways resulted in higher deposition fractions, particularly at the constriction sites, but also at airway bifurcations, while increased mucus thickness provided partial shielding from alpha radiation. However, delayed mucociliary clearance led to longer retention times of radon progeny, increasing cumulative exposure. These findings suggest that dosimetric assessments should account for respiratory conditions, as standard models may not fully reflect the exposure risks for individuals with asthma.

Overall, this work demonstrates the necessity of refining dosimetric models to account for specific characteristics in lung structure and biokinetics. By integrating state-of-the-art modelling approaches, the findings contribute to the improvement of radiation dose assessments for embryos, foetuses, children, and individuals with severe asthma, supporting more accurate evaluations of potential health risks.

Table of content

List of figures

List of Tables

1. Introduction

Assessing radiation doses in specific subpopulations requires models that account for differences in anatomy, physiology, and biokinetics. While general dosimetric models provide estimates for the average adult, significant age- and health-related variations can influence the absorption, distribution, and retention of radionuclides, particularly radon and its progeny. These differences are especially relevant for embryos, foetuses, children, and individuals with asthma, whose physiological characteristics affect internal dose distributions. Understanding these effects is essential for improving risk assessments and refining radiation protection strategies for these potentially vulnerable groups.

For decades, the major concern related to radon exposure focused primarily on male miners inhaling radon and its radioactive decay products. However, epidemiological studies on residential exposure have demonstrated a statistically significant increase in lung cancer risk from prolonged indoor radon exposure (WHO, 2009). Consequently, concerns now extend to both men and women working in offices and facilities located in radon-prone areas, as well as to more vulnerable populations such as pregnant individuals, children, and those with respiratory diseases. These groups may experience different internal exposure patterns due to anatomical and physiological factors affecting radon deposition, retention, and clearance.

Task 3.3 of the RadoNorm project was dedicated to the dose assessment of specific subgroups of the population, focusing on individuals with potentially higher sensitivity to radiation exposure or higher public concern. The work included three key areas. First, a comprehensive model for the dose to the embryo and foetus was developed, starting from the most recent biokinetic models published by the ICRP. The transfer of radioisotopes across the placenta and their distribution in foetal organs were modelled, incorporating gestational changes in maternal and foetal physiology. Second, age-specific dosimetric peculiarities in children were analysed, considering the influence of organ size, morphology, breathing rate, and airway geometry on absorbed dose, particularly in the case of inhaled radionuclides. Finally, the effects of lung diseases on radiation dosimetry were investigated, with a focus on asthma. Computer-based airway models were developed to account for airway remodelling, altered breathing patterns, and mucus dynamics, which affect radionuclide deposition and clearance.

A preprint containing the details of the lung dosimetry work (Füri et al., 2025) is openly available at https://arxiv.org/pdf/2502.19144 . Rather than reproducing its content in full, Chapter 1.2 and 1.3 of this report provide a summarized version of the preprint, which is to be considered part of this deliverable.

1.1 A comprehensive model for the dose to embryo and foetus

Pregnant individuals are a critical group in radiation protection, particularly concerning internal exposure to radionuclides in both occupational and residential exposures. This concern arises from the fetal susceptibility to postconceptional effects of ionizing radiation. Radionuclides can cross the placenta, exposing the foetus directly, and irradiation can also occur due to radionuclide activity in maternal organs (ICRP 2002a).

The ability of radon to cross the placenta was first demonstrated in an animal study by Bagg (1922), in which radon was detected in foetal tissues of pregnant dams. Inspired by these findings, Sikov et al. (1984, 1990) conducted a series of studies investigating the behaviour of the noble gases ^{222}Rn and ^{85}Kr. Their results showed that ^{85}Kr concentrations in foetal tissues were similar to those in maternal tissues, and both gases were able to transfer across the placenta. Additionally, they suggested that radon progeny may also cross the placenta, except for polonium, which tends to accumulate in placental tissue (Sikov & Hui, 1996). As is characteristic of noble gases, when absorbed into the blood, they tend to accumulate in tissues rich in fat (Sakoda et al., 2010). Consequently, maternal and foetal fatty tissues—such as adipose tissue and bone marrow—are of particular interest for radiological protection.

A biokinetic model describes the distribution of a radionuclide in the body over time. These models help in calculating the total transformations in each source region during a specified period (time-integrated activity) (Paquet, 2019). Typically represented by a compartmental structure, the model consists of compartments connected to show radionuclide transfer. This transfer is modelled using differential equations. According to the ICRP, a compartment can represent an organ, part of an organ, tissue, or another substance (ICRP, 2015). The radionuclide activity within a compartment depends on its half-lives and biodistribution. Material transfer between compartments is assumed to follow first-order kinetics, simplifying complex physiological and chemical processes, which is generally adequate for dosimetry and radiation protection (Giussani, 2011).

The most recent age- and sex-specific biokinetic model for radon published in 2023 by Samuels et al (Figure 1) was used for the maternal systemic model. In their model, they assumed that radon transfer rates within the organs follow the Fick's first law of passive diffusion, accordingly to the radon biokinetic model published by the International Commission on Radiological Protection (ICRP) in the Occupational Intakes of Radionuclides (OIR) Part III (ICRP, 2017).

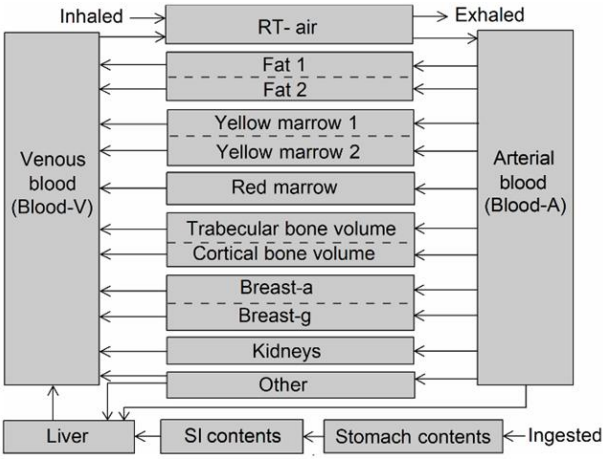

Figure 1. Most recent age- and sex-specific biokinetic model for radon (Samuels et al, 2023).

To assess the foetal uptake of radon, some organs had to be added to the maternal model. The uterus was added to the adult systemic model, the placenta was added as a transfer compartment between the maternal systemic model and the foetal systemic model, and the foetal systemic model was created, containing compartments for the venous and arterial cord blood and some foetal organs relevant for radiation protection (i.e. thyroid, liver, bone surface, bone marrow, lungs, kidneys, and brain). In this scheme, radon that is transferred from maternal blood to the placenta is completely absorbed by the placenta and transferred to the foetal tissues through the venous cord blood. Radon is then washed out from the foetal tissues and goes back to the placenta through the arterial cord blood. The Figure 2 below shows the proposed model for pregnancy with the new compartments depicted in blue.

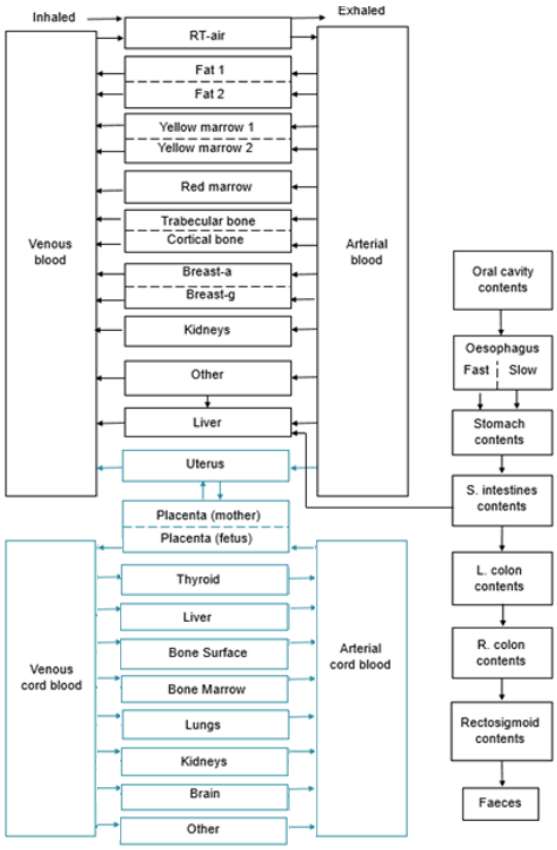

Figure 2 - Proposed biokinetic model for pregnancy.

According to the literature, the placenta is completely developed by the 12th – 15th week of pregnancy (Genbacev et al, 2003). For this reason, the proposed biokinetic model can be applied from the 15th week of pregnancy to term.

Table 1 - Analysis of weight gain during pregnancy (ICRP, 2002b adapted)

Tissues and fluids	**Increase in mass (g) up to**			
	10 weeks	20 weeks	30 weeks	38 weeks
Foetus	5	300	1500	3400
Placenta	20	170	430	650
Uterus	140	320	600	970
Breasts	45	180	360	405
Total	650	4000	8500	12500

During pregnancy, the body undergoes many changes. The ICRP in its publication 89 adopts 12.5 kg as the typical mass gained during pregnancy (Table 1, ICRP, 2002b). The most relevant organs for radon kinetics are the ones consisting of fat, since radon tends to accumulate in tissues rich in fat (i.e. fat 1 and fat 2). Other important changes are those occurring in the breast, uterus, and placenta, due to the increase of mass and blood flow. Table 2 below shows the blood flow to some organs for non-pregnant and pregnant female at term considered by ICRP (ICRP, 2002b).

Table 2 - Reference values for blood flow to selected organs of the non-pregnant and pregnant female near term (ICRP, 2002b adapted).

Organ/tissue	Blood flow rate (% cardiac output)	
	Non-pregnant	Pregnant
Fat	8.5	7.8
Uterus	0.4	12.0
Breast	0.4	3.5
Other	3.2	3.3
Cardiac output (l/min)	5.9	7.3

Along with the maternal body changing with the progress of the pregnancy, the foetus is changing during its development. The three phases of the development are (i) the pre-implantation period, (ii) the embryonic period of organogenesis, and a (iii) foetal period of organ growth. For dosimetric purposes, the pre-implantation and embryonic period are combined and called embryonic period. During this period, that comprises up to 8 weeks after the conception, the dose to the embryo is taken to be the same as the dose delivered to the uterus wall due to its small size (up to 10 g) (ICRP, 2002a). During the early phase of the foetal phase (up to 14–16 weeks of gestation) the absolute growth in foetal mass is relatively small. This phase is followed by a period when the major growth and changes in foetal organs and tissues happen, and it lasts up to 33-34 weeks after gestation (ICRP, 2002a). Table 3 shows the masses for some foetal organs in different ages of gestation in weeks.

Table 3 - Mass of selected foetal tissues at various times of development (ICRP, 2002a adapted)

Organ	Mass (g)						
	8 weeks	10 weeks	15 weeks	20 weeks	25 weeks	30 weeks	38 weeks
Brain	3.7	6.4	22	59	118	192	352
Kidneys	0.022	0.12	1.2	3.5	7.0	12	23
Liver	0.19	0.81	6.1	17	35	59	120
Lungs	0.081	0.53	4.9	12.0	22	32	51
Red marrow	0.065	0.28	2.2	6.5	12	23	47
Bone surface	0.023	0.1	0.76	2.2	4.4	7.3	15
Thyroid	0.011	0.022	0.077	0.18	0.36	0.63	1.3
Total body	4.8	21	160	480	1000	1700	3500

The ICRP has done extensive work to provide reference values that can be applied in dosimetry (ICRP, 2002b). However, reference values for foetal description are not easily found in literature. The blood flow to some foetal organs were provided by Abjudalil et al (2020) in their paper “Fetal Physiologically Based Pharmacokinetic Models: System information on Fetal Cardiac Output and Its Distribution to Different Organs during Development”. In this study, they carried out a literature search to collect and evaluate the changes that the foetal cardiac output and foetal tissue blood flows undergo during the development. The data collected were based on Doppler studies, blood flow through umbilical vein studies, ductus venosus studies, liver veins studies, brain studies, lungs studies and kidneys studies; and they allowed estimating physiologically based reference values. Table 4 shows the foetal blood flow (L/h) to some foetal organs at different gestation week presented by Abjudalil et al (2020).

Table 4 - Foetal blood flow (L/h) at different gestation weeks (mean values, variability ranges in parentheses)
(adapted from Abduljalil, 2020)

Organ blood flow (L/h)	15 weeks	22 weeks	32 weeks	40 weeks
Combined cardiac output	1.52(0.949–2.351)	11.91(7.35–18.45)	49.87 (30.64–77.13)	84.63(52.10–131.69)
Umbilical vein	0.408 (0.254–0.629)	2.820 (1.741–4.368)	9.619 (5.911–14.88)	13.35
Liver	0.310 (0.193–0.477)	2.420 (1.494–3.748)	9.254 (5.686–14.31)	14.02
Brain	0.181 (0.113–0.279)	1.652 (1.020–2.559)	8.010(4.922–12.39)	14.81
Lungs	0.336 (0.209–0.517)	2.620 (1.617–4.059)	10.97 (6.741–16.97)	18.62 ± 11.46–28.97)
Kidneys	0.133 (0.083–0.205)	0.934 (0.577–1.447)	3.294 (2.024–5.095)	4.753 (2.926–7.396)
Bones	0.076 (0.047–0.118)	0.595 (0.368–0.922)	2.493 1.532–3.856)	4.232 (2.605–6.585)

The transfer rates to and from the new compartments were calculated assuming that the transfer of radon among the organs follows the Fick's first law of passive diffusion. Applying this law to a three-compartment model in which radon flows from Compartment A (C_A) through Compartment B (C_B) to Compartment C (C_C), the concentrations of radon in the compartments were calculated considering that the perfusion of radon gas in the tissues is almost instantaneous, what allows the equilibrium between the gas in the blood and in the tissues. The transfer rate from C_A to C_B is calculated by:

$$k_{(C_B,C_A)} = \frac{F}{V_A} \quad (1)$$

being F the blood flow to C_B and V_A the volume of C_A.

The transfer rate from C_B to C_C is calculated by:

$$k_{(C_C,C_B)} = \frac{F}{V_B\, P_{B\to C}} \quad (2)$$

being F the blood flow C_B, and V_B the volume of C_B and $P_{B\to C}$ the partition coefficient for radon from C_B to C_C. This partition coefficient represents the equilibrium concentration ratio of the gas between the compartments.

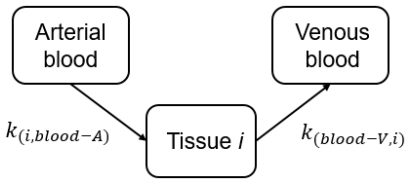

Figure 3 - Three-compartment model composed by the arterial blood, the tissue i, and the venous blood.

Considering a three-compartment model composed by the arterial blood – for inhalation, the gas in the air space is taken to equilibrate with the blood in the lungs (Khursheed, 2000), the tissue *i*, and the venous blood (Figure 3), we can re-write the equations 1 and 2, respectively:

$$k_{(i,blood-A)} = \frac{F_i}{V_{blood-A}} \quad (3)$$

being F_i the blood flow to the tissue *i*, and $V_{blood-A}$ the volume of arterial blood.

$$k_{(blood-V,i)} = \frac{F_i}{V_i P_{i\rightarrow Blood-V}} \quad (4)$$

being F_i the blood flow to the tissue i, V_i the volume of the tissue i, and $P_{i\rightarrow Blood-V}$ the partition coefficient from the tissue i to the venous blood.

Legget et al (2013) in his paper "A generic biokinetic model for noble gases with application to radon" listed tissue-to-blood partition coefficients for radon, xenon, krypton, and argon he gathered from different *in vivo* and *in vitro* studies available in the literature (Legget et al, 2013). Tissue-to-blood partition coefficients for radon necessary to calculate the transfer coefficients from organs to venous blood are listed in Table 5 below.

Table 5 - Estimated partition coefficients for radon for selected organs (Legget et al, 2013 adapted).

Tissue/Blood	Radon
Fat	11
Bone	0.4
Kidney	0.7
Liver	0.7
Brain	0.7
Lung	0.7

The transfer coefficients from arterial blood to the uterus in the maternal model and from venous cord blood to foetal organs (such as the brain, lungs, kidneys, and others) in the foetal model were calculated using Equation 3 for gestational ages of 15, 22, 32, and 40 weeks. Similarly, the transfer coefficients from the uterus to venous blood and from foetal organs (brain, lungs, kidneys, and others) to arterial cord blood were calculated using Equation 4 for the same gestational ages. The transfer rates for the placenta, venous cord blood, and arterial cord blood were determined based solely on blood flow, as these were not included in the three-compartment models. For foetal tissues like the bone marrow, thyroid, bone surface, and liver, where no sufficient data was available to apply the equations directly, the transfer rates were calculated using mass ratios relative to the "other" foetal compartment at the different gestational ages (15, 22, 32, and 40 weeks).

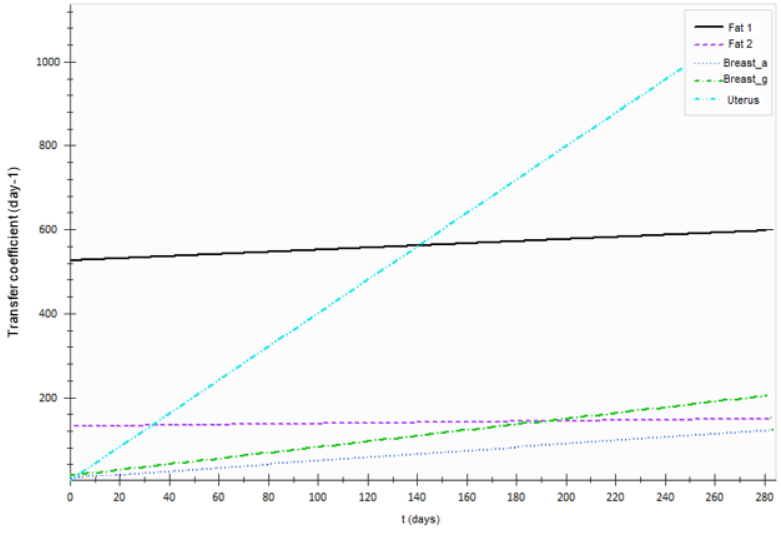

Figure 4 - Changes in the transfer coefficients from arterial blood to some maternal tissues for different gestation ages in days.

Due to changes in tissue mass and blood flow in both maternal and foetal tissues, the transfer coefficients for certain maternal tissues (e.g., fat, breast, and uterus) and foetal tissues vary over time. Therefore, these transfer coefficients are time-dependent and they are described by analytical functions built on the reference values available for selected gestational ages (15, 22, 32, and 40 weeks). Figures 4 and 5 show the changes of the transfer coefficients from arterial blood to some maternal tissues (Figure 4) and from the venous cord blood to some foetal tissues, respectively (Figure 5).

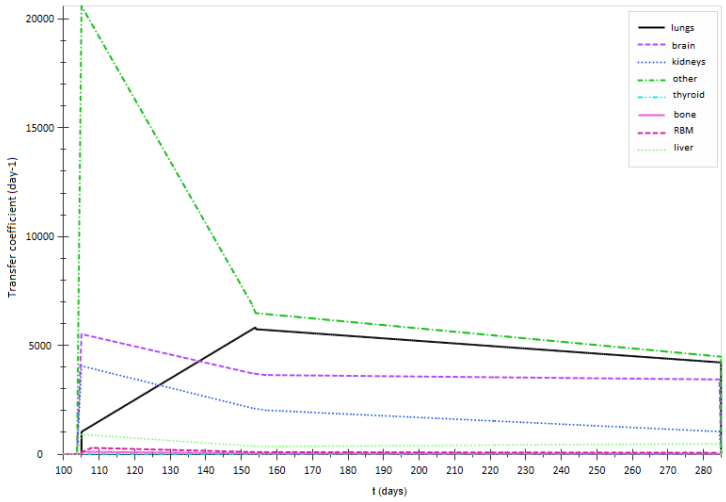

Figure 5 - Changes in the transfer coefficients from the venous cord blood to some foetal tissues for different gestation ages in days.

The biokinetic model was implemented using the software SAAM II (Nanomath LLC, Spokane, USA). For acute exposures, only up to 0.001% of the intake reaches foetal tissues. While the direct transfer of radon to foetal tissues is limited, the contribution of radon progeny must also be considered, as these decay products may have longer retention times and present additional radiation exposure risks.

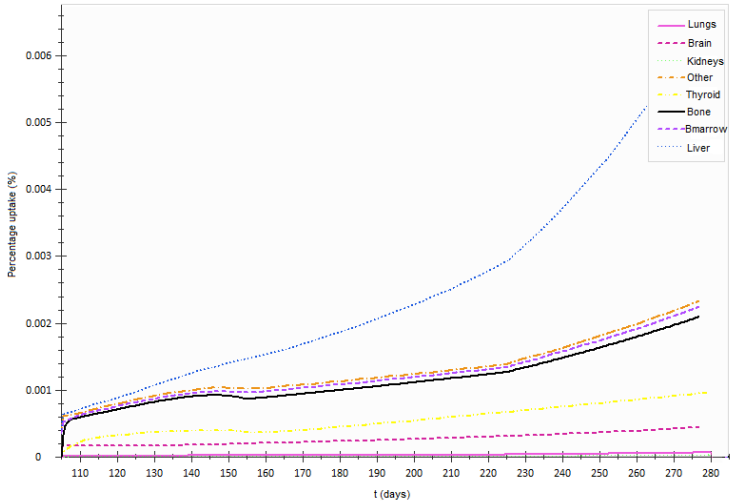

Figure 6 - Percentage of radon uptake in fetal tissues after chronic intakes.

In contrast, chronic exposure to radon, which is more likely to occur in individuals living or working in radon-prone areas, can lead to a gradual increase in radon activity within foetal tissues throughout pregnancy. Our model also showed that the foetal liver receives the highest radon concentration (Figure 6), likely due to foetal circulation, which includes a shunt directing a significant portion of blood flow to the liver. Additionally, foetal red bone marrow is of great interest in radiation protection because it is a

fatty tissue typically surrounded by bones, which can accumulate radon progeny, particularly ^{210}Pb —a long-lived alpha-emitting radionuclide.

A manuscript detailing the model and its transfer coefficients is currently in preparation for publication. A poster presenting the state of the art was submitted to the ICRP 2021+1 Symposium, and a short paper was published in the conference proceedings (ICRP, 2023). More recently, at the ICRP 2023 Symposium, this work was recognised as a finalist for the ICRP Cousins Award for Young Researchers in Radiation Protection, highlighting its contribution to the field.

Regarding radon progeny, the main focus is on polonium (Po), lead (Pb), and bismuth (Bi), as they contribute the most to internal exposures. Other radionuclides in the radon decay chain, such as thallium (Tl), mercury (Hg), and astatine (At), were not considered due to their very short physical half-lives or the extremely low probability of radon decay leading to their formation (~0.002%). Lead behaves analogously to calcium, allowing for its translocation from maternal bones to foetal bones during pregnancy, which raises questions about its contribution to foetal bone marrow doses (Richardson, 1994). Similarly, based on animal studies, only a small fraction (~10%) of Po and Bi crosses the placenta and reaches the foetus (Richardson, 1992).

The publication, "Contribution of Maternal Radionuclide Burdens to Prenatal Radiation Doses," (Sikov and Hui, 1996) provides valuable insights into how radionuclides, such as lead (Pb), polonium (Po), and bismuth (Bi), are distributed and retained in the foetus. The data, presented in Appendix A of the publication, includes estimates of fractional deposition at various stages of pregnancy, considering the maternal and foetal compartments. These models, primarily based on ICRP Publications 30, 48, 53, 56, and 67, were updated to account for the specific conditions of pregnancy, such as placental transfer and the movement of radionuclides into the foetus. The model assumes an instantaneous introduction of activity, with fractions distributed between the maternal blood, uterus, placenta, and the developing foetus.

Building on Sikov's work, we adapted his data to refine a biokinetic model specifically for radon progeny. We adopted the ICRP most recent adult models for Pb, Po, and Bi for the maternal systemic model and introduced additional compartments for the uterus, placenta, and foetal tissues. By incorporating the fractional deposition data from Sikov's tables, we adjusted the transfer coefficients to better reflect the distribution of radionuclides at different points during pregnancy. In addition, we developed fitting curves to model how radionuclides were retained in the fetus over time, based on Sikov's time-point data. These curves allowed us to better understand how the distribution of activity changes throughout pregnancy and provided a clearer picture of radionuclide retention in foetal tissues. All assumptions, model descriptions, and transfer coefficients for Po, Pb, and Bi are being compiled into another publication currently in preparation for submission.

For a detailed assessment of foetal radiation exposure Specific Absorbed Fractions (SAFs) for the foetal organs are required. SAFs, as defined by the ICRP, represent the fraction of energy emitted by a radioactive source in a specific organ or tissue that is absorbed by a target tissue (ICRP, 2007). Researchers at Hanyang University, Korea, which develop the reference pregnancy model for ICRP, have collaborated with us and are finalising the calculation of the SFAs for the foetal source regions that were included in our models and that will be used for the dose assessment.

In conclusion, the added value of this work lies in its comprehensive approach to understanding and modelling the biokinetics of radon and progeny. By developing detailed biokinetic models for individual elements of the radon and thoron decay chains, this work provides a versatile tool for analysing the distribution and retention of these radionuclides in foetal compartments. The dose coefficients derived from this research will offer essential data for evaluating the potential radiation exposure to the foetus, which can be applied in risk assessments and radiation protection guidelines. This combination of biokinetic modelling and dose coefficient calculation not only advances the scientific understanding of

radon progeny in pregnancy but also contributes significantly to improving safety standards and ensuring more accurate radiation dose estimations for pregnant women.

1.2 Dosimetric peculiarities of children of different ages

To analyse the influence of individual characteristics on radon progeny deposition and radiation burden, we employed the Stochastic Lung Model (SLM), a computational tool designed to simulate the transport, deposition, and clearance of inhaled particles within the human respiratory tract. The model was adapted to represent three distinct subject groups: a healthy adult, a five-year-old child, and an adult with severe asthma. Key morphological and physiological parameters, including airway geometry, tidal volume, breathing frequency, mucus thickness, and mucociliary clearance rates, were incorporated to capture the differences between these groups. The model was further enhanced with alpha-particle microdosimetry, allowing us to estimate the absorbed dose in basal and secretory cell nuclei, which are the primary targets for radiation-induced effects. We simulated exposure under typical indoor radon concentrations, ensuring that the results are applicable to real-world scenarios.

The simulations indicated that children experience a higher absorbed dose in basal and secretory cell nuclei of the bronchial epithelium despite having a lower total deposition of radon progeny compared to adults. This outcome is primarily due to their smaller airway dimensions, which result in a higher concentration of deposited particles per unit surface area. Since the range of alpha particles is short, the proximity of these deposited particles to sensitive lung cells increases the localised radiation dose. Although children inhale fewer particles overall due to their smaller lung capacity, their airway structure leads to a relatively higher dose at the cellular level. These findings suggest that age-specific anatomical differences should be considered in radiation risk assessments, as conventional models based on adult lung parameters may not fully account for exposure risks in younger individuals.

Another important factor influencing radiation dose in children is mucus layer thickness, which serves as a protective barrier against direct radiation exposure. Compared to adults, children have thinner mucus layers, reducing this shielding effect and allowing a greater fraction of alpha radiation to reach the basal and secretory cell nuclei. Their higher breathing rates also affect deposition dynamics and clearance efficiency, potentially influencing dose distribution in the bronchial tree. Although faster breathing does not necessarily increase total deposition, it impacts how long particles remain in the lungs and how they are transported within the airways. Given that basal and secretory cells play a key role in radiation-induced carcinogenesis, these findings suggest that children may require more detailed dose assessments in radon exposure studies. Standard dosimetric models typically assume uniform risk across age groups, but our results indicate that age-specific dose calculations could improve risk estimates for younger populations. Further investigation is needed to determine how these anatomical and physiological factors influence the biological response to long-term radon exposure.

1.3 The effects of lung diseases on absorbed dose and dose distribution in the lung

While lung morphology influences radon progeny deposition in children, it also plays an important role in individuals with chronic respiratory conditions, particularly severe asthma. Airway constriction, a defining feature of asthma, affects the deposition pattern of inhaled particles. In severe asthma, airway constriction may be present permanently, not only during attacks. In addition, airflow split among the different lung lobes is modified in severe asthmatics. Our results show that narrowed airways and modified airflow distribution in asthmatic individuals lead to increased deposition fractions, particularly in the bronchial epithelium, where airflow patterns enhance particle deposition at airway bifurcations. The increased deposition in these regions suggests that, similar to the case of children, the absorbed dose per unit surface area is elevated compared to a healthy adult lung. However, while in children this

effect is primarily a result of anatomical scaling, asthmatic lungs exhibit a more complex interaction between deposition, mucus properties, and clearance efficiency.

One important finding in asthmatic individuals is the role of mucus thickness and clearance rates in determining the absorbed radiation dose. Unlike children, who have a thinner mucus layer that provides limited shielding, individuals with severe asthma often develop excessive mucus production, leading to a thicker barrier. This additional mucus can provide some attenuation of alpha radiation by increasing the distance between deposited particles and sensitive cell nuclei. However, this effect is counteracted by impaired mucociliary clearance, which is a common feature of severe asthma. In healthy lungs, mucus and trapped particles are continuously transported out of the airways by ciliary motion. In individuals with asthma, this process is slower, leading to longer retention times of radon progeny in the bronchial epithelium. The combination of increased deposition and prolonged retention suggests that individuals with asthma may experience a greater cumulative radiation burden, despite the partial shielding effect of the thicker mucus.

These results suggest that standard radiation risk models, which assume normal lung function, may not fully account for the dose received by individuals with asthma. The interaction between airway narrowing, mucus properties, and particle retention highlights the need for further refinement of dosimetric assessments for individuals with chronic lung conditions. Given that asthma is associated with localized inflammation and epithelial remodelling, it is important to investigate whether prolonged exposure to radon progeny has additional implications in this population. Our findings indicate that individuals with asthma should be considered separately in radiation risk assessments, particularly in occupational settings where radon exposure is significant. Further research could explore whether medical treatments aimed at improving mucus clearance reduce the overall radiation burden in individuals with asthma.

2. Conclusions

The assessment of radiation doses in specific subpopulations, including embryos, foetuses, children, and individuals with lung diseases, highlights the importance of incorporating individual anatomical, physiological, and biokinetic characteristics into dose calculations. Standard dosimetric models, typically based on adult physiology, may not fully capture the exposure risks faced by these groups. By refining computational models, this study provides a more detailed understanding of radiation dose distribution in these specific populations.

For embryos and foetuses, a biokinetic model for radon exposure during pregnancy was developed to evaluate maternal-to-foetal transfer of radon and its progeny. This model includes the placenta as a transfer compartment and incorporates foetal organs such as the liver, lungs, kidneys, and brain. The findings indicate that while the direct transfer of radon gas to foetal tissues is limited, radon progeny, particularly lead and polonium, may contribute more significantly to the foetal radiation burden. The foetal liver was identified as the primary site of radon accumulation, likely due to foetal circulation patterns. Additionally, red bone marrow is of particular interest due to the retention of lead, which may result in long-term internal exposure. The study also introduced time-dependent transfer coefficients to account for gestational changes in maternal and foetal physiology, improving the accuracy of foetal dose estimations.

For children, numerical dosimetry models revealed that smaller airway dimensions and thinner mucus layers lead to a higher absorbed dose in the basal and secretory cell nuclei of the bronchial epithelium, despite lower total deposition of radon progeny compared to adults. The higher concentration of deposited particles per unit surface area increases energy deposition in these sensitive lung tissues. Additionally, age-dependent differences in breathing patterns and airway morphology were found to influence dose distributions, emphasising the need for age-specific risk assessments in radiation dosimetry. Since basal and secretory cells are associated with radiation-induced lung cancer risks, these

findings suggest that current generalised dosimetric models may underestimate the potential health risks for children.

For individuals with severe asthma, computational airway models demonstrated that airway constriction and mucus hypersecretion significantly alter radon progeny deposition and clearance. The narrowed airways in asthmatic individuals resulted in higher deposition fractions, particularly at airway the constriction sites and at airway bifurcations. Although increased mucus thickness provided some shielding from alpha radiation, the delayed mucociliary clearance led to a longer retention time of radioactive particles, increasing cumulative exposure. These findings suggest that radiation dose assessments should consider respiratory conditions, as deposition and clearance mechanisms in asthmatic lungs differ from those in healthy individuals.

Overall, this work highlighted the necessity of refining dosimetric models to account for individual variability in lung structure and biokinetics. Future efforts should focus on further validation of these models with experimental data, as well as incorporating uncertainty analyses to improve model reliability. The findings contribute to a better characterisation of radiation dose distributions in embryos, foetuses, children, and individuals with asthma, supporting more accurate dose estimations in these populations.

3. References

Abduljalil, K. Pan, X. Clayton, R. Johnson, T. N. Jamei, M. Fetal Physiologically Based Pharmacokinetic Models: Systems Information on Fetal Cardiac Output and Its Distribution to Different Organs during Development. Clinical Pharmacokinetics. 2021. 60:741–757.

Bagg, M. R. 1922. Disturbances in mammalian development produced by radium emanation. Am J Anat 30:133.

Degenhardt, Ä.L., Giussani, A., Madas, B.G., 2023. A comprehensive biokinetic model for the dose to embryo and fetus due to radon intakes by the mother – Part I: the state of the art. Ann ICRP 52:142–147.

Füri, P., Farkas, Á., Hofmann, W., Madas, B.G., 2025. The role of individual characteristics of human subjects on the radiation burden of the bronchial airways from radon progeny. https://doi.org/10.48550/arXiv.2502.19144

Genbacev, O., et al. 2003. Regulation of human placental development and its impact on fetal growth. Journal of Reproductive Immunology, 59(1-2), 121-135.

Giussani, A. Uusijärvi, H., 2011. Biokinetic Models for Radiopharmaceuticals. In: Cantone, M.C., Hoeschen, C. (Eds.), Radiation Physics for Nuclear Medicine. Springer, Berlin.

ICRP, 2002a. Doses to the embryo and fetus from intakes of radionuclides by the mother. ICRP Publication 88. Ann. ICRP 31 (1–3).

ICRP, 2002b. Basic Anatomical and Physiological Data for Use in Radiological Protection: Reference Values. ICRP Publication 89. Ann. ICRP 32 (3-4).

ICRP, 2007. The 2007 Recommendations of the International Commission on Radiological Protection. ICRP Publication 103. Ann. ICRP 37 (2–4).

ICRP, 2015. Occupational intakes of radionuclides: Part 1. ICRP Publication 130. Ann. ICRP 44(2).

ICRP, 2017. Occupational intakes of radionuclides: Part 3. ICRP Publication 137. Ann. ICRP 46(3/4).

Khursheed, A., 2000. Doses to systemic tissues from radon gas. Radiat. Prot. Dosim. 88, 171–181.

Leggett, R., Marsh, J., Gregoratto, D., Blanchardon, E., 2013. A generic biokinetic model for noble gases with application to radon. J. Radiol. Prot. 33, 413.

Paquet, F., 2019. The new ICRP biokinetic and dosimetric models. BIO Web Conf. 14, 02001.

Richardson, R.B., 1992. Transfer of Radiobismuth to the Fetus in Guinea-Pigs. Radiat. Prot. Dosimetry 41, 169–172.

Richardson, R.B., 1994. Model of 210Pb and 210Po placental transfer to fetal bone. Radiat. Prot. Dosimetry 54, 139–144.

Sakoda, A., Ishimori, Y., Kawabe, A., Kataoka, T., Hanamoto, K., Yamaoka, K., 2010. Physiologically based pharmacokinetic modeling of inhaled radon to calculate absorbed doses in mice, rats, and humans. J. Nucl. Sci. Technol. 47, 731–738.

Samuels, C. Marsh, J. Legget, R. 2023. An age- and sex-specific biokinetic model for Radon J. Radiol. Prot. 43 041502.

Sikov, M., Ballou, J. E. Willard, D. H. Andrew, F. D. 1984. Disposition and Effects of 85Kr in Pregnant Rats. Health Physics 47. No. 3 417-427.

Sikov, M.R., Cross, F.T., Mast, T.J., Palmer, H.E., James, A.C., Thrall, K.D., 1990. Developmental toxicology of radon exposures. Indoor Radon and Lung Cancer: Reality or Myth? Part II. Battelle Press, Columbus, OH.

Sikov, M.R., Hui, T.E., 1996. Contribution of Maternal Radionuclide Burdens to Prenatal Radiation Doses. Nuclear Regulatory Commission, Washington, DC.

World Health Organization. 2009. WHO handbook on indoor radon: A public health perspective. World Health Organization.